metals

MDPI

Review

WO_3 and Ionic Liquids: A Synergic Pair for Pollutant Gas Sensing and Desulfurization

Francesca D'Anna [1,*], Maria Luisa Grilli [2,*], Rita Petrucci [3] and Marta Feroci [3,*]

[1] Dept. STEBICEF, University of Palermo, Viale delle Scienze, Build. 17, 90128 Palermo, Italy
[2] Italian National Agency for New Technologies, Energy and Sustainable Economic Development (ENEA), Energy Technology Department, Casaccia Research Center, Via Anguillarese 301, 00123 Rome, Italy
[3] Dept. Fundamental and Applied Sciences for Engineering (SBAI), Sapienza University of Rome, via Castro Laurenziano, 7, 00161 Rome, Italy; rita.petrucci@uniroma1.it
* Correspondence: francesca.danna@unipa.it (F.D.A.); marialuisa.grilli@enea.it (M.L.G.); marta.feroci@uniroma1.it (M.F.); Tel.: +39-23-897540 (F.D.A.); +39-06-41733132 (M.L.G.); +39-06-49766563 (M.F.)

Received: 9 March 2020; Accepted: 2 April 2020; Published: 4 April 2020

Abstract: This review deals with the notable results obtained by the synergy between ionic liquids (ILs) and WO_3 in the field of pollutant gas sensing and sulfur removal pretreatment of fuels. Starting from the known characteristics of tungsten trioxide as catalytic material, many authors have proposed the use of ionic liquids in order to both direct WO_3 production towards controllable nanostructures (nanorods, nanospheres, etc.) and to modify the metal oxide structure (incorporating ILs) in order to increase the gas adsorption ability and, thus, the catalytic efficiency. Moreover, ionic liquids are able to highly disperse WO_3 in composites, thus enhancing the contact surface and the catalytic ability of WO_3 in both hydrodesulfurization (HDS) and oxidative desulfurization (ODS) of liquid fuels. In particular, the use of ILs in composite synthesis can direct the hydrogenation process (HDS) towards sulfur compounds rather than towards olefins, thus preserving the octane number of the fuel while highly reducing the sulfur content and, thus, the possibility of air pollution with sulfur oxides. A similar performance enhancement was obtained in ODS, where the high dispersion of WO_3 (due to the use of ILs during the synthesis) allows for noteworthy results at very low temperatures (50 °C).

Keywords: WO_3; ionic liquids; gas sensor; pollutant gases; desulfurization

1. Introduction

Tungsten trioxide (WO_3) is a n-type semiconductor widely investigated both in its doped and undoped forms, in powders, films and nanostructures, because of its good gas sensing, antibacterial and antimicrobial properties, its pH sensitivity, its photocatalytic activity for water-splitting, etc. A wide range of applications in several technological areas such as photocatalysis [1–3], gas sensing [4–8] and electrochromism [9–14] has been demonstrated. The reason for such wide applications lies in the semiconducting properties of WO_3, its polymorphous structure, its optical characteristics and its wide band gap. Tungsten trioxide shows several temperature dependent phase transitions: at room temperature, and up to 133 °C, the stable phase is the monoclinic one I (γ-WO_3). Upon heating above 330 °C, γ-WO_3 is converted to orthorhombic β-WO_3, which is stable up to 740 °C. At $T > 740$ °C the tetragonal α-WO_3 phase is found. A metastable phase, the hexagonal WO_3 (h-WO_3) may also be obtained by opportune chemical synthesis [15,16] with potential advantages over the larger band gap γ-WO_3 phase [17]. In WO_3 powders, doped with H, Na, Li or other impurity atoms or in WO_3 thin film form, the cubic c-WO_3 phase also occurs [18,19]. This cubic phase is considered as the ideal high temperature phase and is consequently used as the reference for the structure of WO_3 [20]. The cubic perovskite-like structure is shown in Figure 1 and consists of corner sharing of regular octahedra with oxygen atoms at the corners and tungsten atoms at the center of each octahedron.

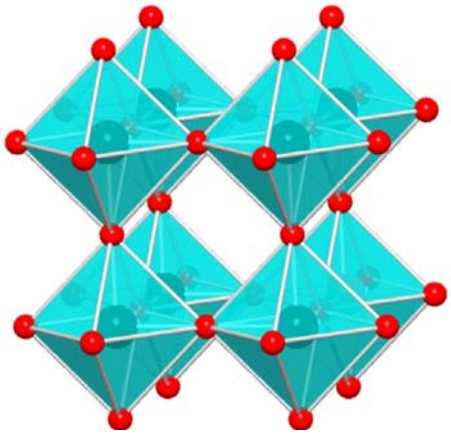

Figure 1. WO_3 cubic structure. Reproduced with permission [20]. Copyright 2019, Wiley.

The electronic bandgap value for WO_3 has been found in the range 2.6–3.3 eV, depending on the WO_3 phase and microstructure [9,21,22].

Together with SnO_2, WO_3 is the most widely used metal oxide semiconductor in commercial sensors due to its high sensitivity. Good sensing performances have been largely demonstrated for NO_x gas [23–27], but good detection of NH_3 [28,29], H_2S [30], H_2 [31] and SO_2 [32] was also demonstrated. In addition, due its good catalytic properties, WO_3 was also used as the metal oxide auxiliary phase in high temperature electrochemical sensors for NO_2 and CO detection [5] and for on board diagnostic (OBD) [33,34].

The gas sensing mechanism of metal oxide semiconductors is due to the resistivity changes in the presence of the adsorbed gas. According to Yamazoe and Shimanoe [35], the power laws that describe the change in semiconductors' resistance under exposure to a target gas can be derived by combining a depletion theory of semiconductors, which deals with the distribution of electrons between surface state (surface charge) and bulk, with the dynamics of adsorption and/or reactions of gases on the surface, which is responsible for the accumulation or reduction of surface charges. The role played by the negatively charged oxygen adsorbates on the sensing characteristic of the semiconductor gas sensors is the most extensively accepted explanation. In air the surface of a metal oxide is covered by several oxygen adsorbates such as O_2^-, O^- and O^{2-}. In the case of n-type semiconductors, these oxygen adsorbates build a space-charge region on the surface of the metal oxide grains, resulting in an electron-depleted surface layer due to the electron transfer from the grain surface to the adsorbates. The depth of the space-charge layer is a function of the surface coverage of oxygen adsorbates and intrinsic electron concentration in the bulk.

The resistance of an n-type semiconductor gas sensor in air is rather high due to the development of a potential barrier to electronic conduction at each grain boundary. In the presence of a reducing gas, free charge carriers are released to the conduction band, whereas the reaction product desorbs thermally from the semiconductor. The electrons trapped by the oxygen adsorbates are transferred back to the oxide grains leading to a decrease in the potential barrier height and a resistance drop, as depicted in Figure 2 [36].

The resistance of a metal oxide semiconductor, and therefore its sensing properties, is affected by the depth of the space charge region L and by the crystallite size D of the material, as shown in Figure 3. The sensor element may be described as consisting of a chain of uniform crystallites of size D connected to each other by the necks of grain boundaries. Depending on the relative size of D and L, three different cases may occur [37]. If D is much greater than 2L (D >> 2 L), most of the volume of the crystallite is unaffected by the surface interaction, and resistivity is dominated by grain boundaries. When D > 2L, the grain size decrease in the depletion region extends deeper into the grains and the resistivity is controlled by the neck between grains.

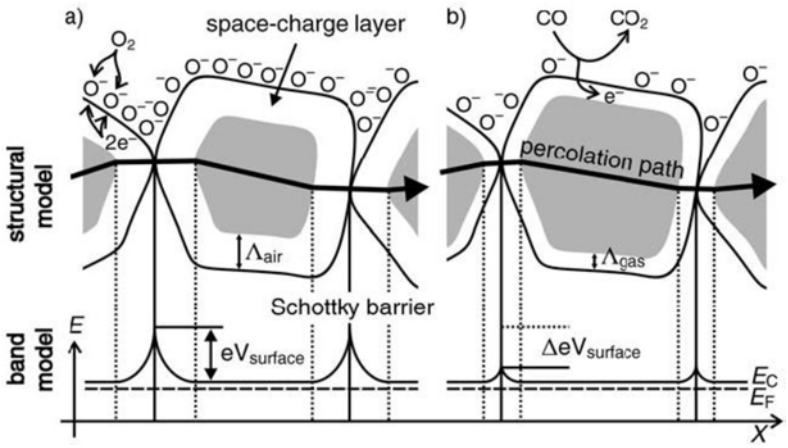

Figure 2. Structural and band models of conductive mechanism in n-type metal oxide semiconductor upon exposure to target gas, (**a**) with or (**b**) without CO [36].

When D < 2L the depletion region extends in the whole grain, the crystallites are almost fully depleted of electrons and resistance is dominated by the grain size effect. In this latter case of grain control sensing mechanism with a higher sensitivity and therefore a higher gas response are observed with respect to the other two cases, because of the larger quantity of adsorbates which can react with the target gas. The use of ultrafine grains of D comparable with or less than 2L is to achieve the state where the transducer function of the elements is operated by the grain-control mechanism [37].

It is therefore extremely important to reduce the calcination temperatures of the materials and/or the operating temperature of the gas sensor to avoid grain size increase. The morphology of the semiconducting oxide also plays a fundamental role in gas sensing performances. Each morphology has its own advantages, contributing to increased active sites on the surface, accelerated response speeds and enhanced gas diffusion. Among the various morphologies, hollow nanostructures and core-shell nanostructures show superior performances due to their larger specific surface areas, which allow both the inner and the outer surface to absorb the target gases [38].

The gas sensing of many WO_3 nanostructures has been investigated: nanoparticles, nanospheres [39,40], nanosheets [41], nanorods [42], nanowires [43,44]. In addition, doping with noble metals (Au, Ag, Pt and Pd) effectively enhances the catalytic properties of WO_3 and metal oxide semiconductors [45].

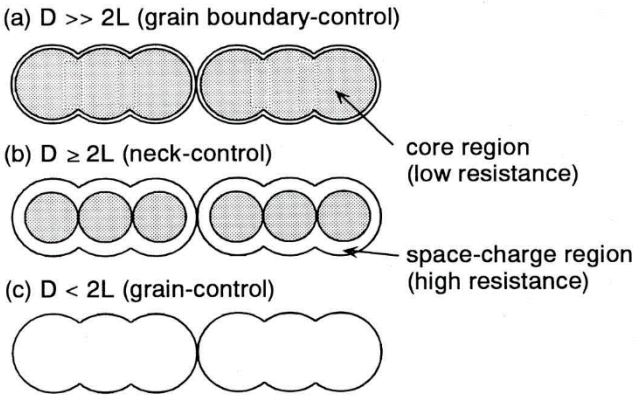

Figure 3. Schematic model of the grain size effect on a metal oxide semiconductor. Grain is represented by grey colour and depletion layer by white colour. Reproduced with permission [37]. Copyright 1991, Elsevier.

Several methods have been reported for the synthesis of WO_3 powders and nanostructures, such as thermal decomposition [46], precipitation [47], hydrothermal synthesis [48–50], electrodeposition [51], sol gel [52], etc.

Thin WO_3 films are usually grown using physical vapor deposition (PVD) techniques such as radio frequency sputtering [10,53], pulsed laser deposition [54], thermal [55] and e-beam evaporation, [56] or chemical vapor deposition (CVD) [57].

Ionic Liquids

Ionic liquids (ILs) have been known about since the late 1980s. They have been defined as salts having melting temperatures below 100 °C [58]. This general definition includes the more specific one related to room temperature ionic liquids (RTILs), i.e., salts liquid at room temperature. As a consequence of the above feature, RTILs can be used as solvents, and since their first appearance in literature, they have been claimed as an eco-friendly alternative to conventional organic solvents. ILs are formed by organic cations and organic or inorganic anions (Scheme 1).

Cations:

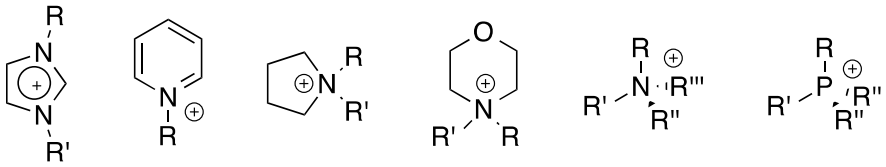

Anions:

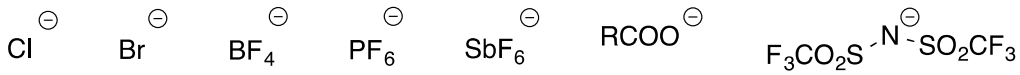

Scheme 1. Structures of most common cations and anions.

This endows them with low vapor pressure and flammability and high thermal stability. Consequently, their use allows all environmental issues generally deriving from the volatility of organic solvents to be avoided. The above-mentioned properties heavily depend on the cation or anion structure. On this subject, the melting point is determined by ion symmetry, as well as by the length of the alkyl chain on the cation. Properties like density and viscosity are affected, beyond the alkyl chain length, also by the cation hydrogen bond donor or the anion coordination ability. The latter feature also influences ILs thermal stability [59,60].

ILs also show high solubilizing ability and, being formed only by ions, high conductivity. The first feature explains why ILs have been applied in different fields of chemistry research. Indeed, they are able to dissolve both organic and inorganic small solutes, but also polymeric materials. In the latter case, they proved very efficient in dissolving natural polymers hard to solubilize in water or organic solvents, like cellulose and lignin [61,62].

Thanks to their conductive behavior they have been widely used in electrochemistry, in the preparation of lithium batteries, but also as electrolytes in dye sensitized solar cells. In some of the above-mentioned applications, IL use is advantageous with respect to inorganic electrolytes, as a consequence of their lower corrosivity [63,64].

Notwithstanding the plethora of different applications, the use of ILs as reaction media is probably the most widely applied and investigated [65–70]. They have been used to perform classical organic reactions, such as nucleophilic aromatic substitution, elimination reaction, ring to ring interconversion in heterocyclic systems, cycloaddition reaction and so on [71–77].

Interestingly, ILs, and in particular imidazolium-based ILs, proved very efficient in performing organocatalyzed reactions, taking advantage from the high activity of electrogenerated *N*-herocyclic carbenes [78–83].

As far as inorganic materials are concerned, ILs also interact well with metallic species and, in this context, their use in combination with metal oxides, with the aim to obtain efficient catalytic systems or sensors, is a very active area of research.

To this aim, they have been used to obtain gas sensors [84], but also to prepare noble metal clusters to be used in alcohol oxidation processes [85]. Independently from the nature of the processes in which they are used, ILs are frequently able to improve performance of processes. Indeed, they are able to increase both yield and reaction rates, but in some cases, they are also able to decrease the temperature of the processes. All the above effects allow their classification as valuable alternative to conventional solvents to be justified.

All of the above advantageous effects are generally explained taking in consideration the ionic nature of these solvents and considering the possibility to tailor properties of ILs to the features of the performed processes. Indeed, the behavior of ILs can be significantly changed, bringing small variations to cation or anion structures.

On this subject, it is worth noting that two different points of views are frequently detected in literature about the effect of ILs, as reaction media. The first one considers ILs as salt solutions and explains the effect using classical solvent parameters [86–88]. Differently, in some other cases, above all in the presence of aromatic ILs, the effects are rationalized considering the supramolecular network that features these solvents, justifying their description as polymeric supramolecular fluids [89,90].

In addition to simple ILs, task specific ionic liquids (TSILs) must also be considered. In this case a catalytic function borne on the cation or anion structure endows the salt not only with solvent but also catalyst function [85,91,92].

Irrespective of the nature and function of the IL, one of the most important advantages in using ILs lies in the possibility of their reuse, as simple liquid-liquid extraction allows the solvent/catalyst to be obtained in its pure form, ready for recycling. Clearly, the above aspect is relevant not only from an economical point of view, but above all from an environmental point of view. Indeed, in many cases they can be reused for at least five cycles, inducing a small decline in the degree of solution, as observed in the phosphorylation of corn starch using 1-butyl-3-methylimidazolium chloride as solvent medium [93].

Other systems that allow efficient IL recycling are the supported ionic liquid phases (SILPs) [94–96] or systems in which ILs are immobilized in a gelatinous network, giving rise to the obtainment of the so-called ionogels [97–101].

Besides the applications, the biological and environmental effects of these solvents have also been recently addressed to minimize the impact at the time of disposal. The tailoring property is very useful also in this context. Indeed, a suitable choice of substituents on the cation or anion structure allows the impact of these solvents to be significantly decreased, both on the environment and human health [102]. On this subject, aliphatic cations are generally preferred to aromatic ones, and among the anions, the ones deriving from amino acids, alkyl sulphates, halides and sugar-based anions are considered the most environmentally friendly [103].

Lastly, biobased ILs have also recently played a pivotal role. Indeed, the possibility of preparing these solvents using waste materials represents a way to improve their life cycle [104]. Indeed, several building blocks, including sugars, aminoacids, amino alcohols and so on, can be used as a precursor of ILs, and biobased ILs are solvents that should be suitable for processing their starting material. This, as recently reported by Socha et al., should allow a closed-loop biorefinery able to satisfy its own need of solvent to be realized [105].

As previously stated, ILs can be successfully used in various application fields. The synergic effect of WO_3 and ionic liquids in gas sensing and desulfurization reactions has been only recently studied, and this can be attributed to the ability of ILs to dissolve inorganic compounds (thus allowing the

production of composites with a high active area) and to the solubility of water and permeability of some gases in certain ionic liquids, thus allowing the concentration of analytes (gases) on the surface of the sensor, while lowering the negative effect of high levels of humidity (vide infra).

We herein want to review the contextual and synergic use of WO_3 and ionic liquids in the field of air pollution, from the point of view of the quantification of gaseous air contaminants (pollutant gas sensing, paragraph 2) and from the point of view of the possibility of decreasing the extent of SO_x liberation in the atmosphere due to impure fuel combustion (hydrodesulfurization and oxidative desulfurization, paragraph 3).

2. WO_3 and Ionic Liquids in Pollutant Gas Sensing

Air quality assessment is one of the main tasks of recent (and future) years. In fact, "Air pollution kills an estimated seven million people worldwide every year. WHO data show that 9 out of 10 people breathe air containing high levels of pollutants. WHO is working with countries to monitor air pollution and improve air quality" [106]. In particular, air pollution can be divided into two different categories (based on ambient and pollution source): indoor and outdoor. Indoor (household) air pollution is mainly due to incorrect fuel utilization (in cooking or stoves), while outdoor (ambient) air pollution has a larger number of sources [107]:

- Fuel combustion from motor vehicles (e.g., cars and heavy-duty vehicles),
- Heat and power generation (e.g., oil and coal power plants and boilers),
- Industrial facilities (e.g., manufacturing factories, mines and oil refineries),
- Municipal and agricultural waste sites and waste incineration/burning,
- Residential cooking, heating and lighting with polluting fuels.

It is thus evident that cheap, light, easy-to-use, non-polluting and/or recyclable gas sensors are the topic of current research [108,109]. One of the main differences between indoor and outdoor gas sensing is the very different level of humidity of these two ambients, very high outdoor and controllable indoor. High levels of humidity can compromise the operations of the sensor devices [110].

Many are the materials used in air pollutant sensors, and among them semiconducting metal oxides are very popular [111]. In particular, WO_3, due to its peculiarities, is often used as sensor material [112–115].

More recently, in order to enhance the performance of WO_3 sensors, ILs have been used both in the WO_3 production process (i.e., incorporating ILs in WO_3 structures or influencing such a structure) and in the sensor device construction process (i.e., incorporating ILs in the device). In both cases better performances were obtained in comparison to the same sensors obtained without using ILs.

Li and coworkers reported the use of two very common imidazolium ILs (1-butyl-3-methylimidazolium and 1-carboxymethyl-3-methylimidazolium chlorides, BMImCl and CMImCl, respectively) in the synthesis of nanostructured WO_3 particles [116]. In particular, nanorods could be selectively obtained using 1-carboxymethyl-3-methylimidazolium chloride, while nanoparticle-constructed spheres could be selectively obtained using 1-butyl-3-methylimidazolium chloride, in both cases starting from WCl_6.

The effect of the nature and amount of imidazolium ionic liquids on the morphology of the produced nanoparticles was evidenced, and a hypothesis of mechanism was reported. In all cases, starting from WCl_6 as tungsten source and after calcination, monoclinic WO_3 was obtained, in pure form and well crystallized, but in the absence of IL, nanoplates were obtained (1 hundred nm size), while in the presence of CMImCl nanorods (30 nm diameter), and in the presence of BMImCl, spheres (1500 nm size, formed by subunits of 40 nm size) were obtained. The morphology of produced nanostructured WO_3 not only depends on the nature of the substituents on the imidazolium cation (butyl or carboxymethyl), but also on the amount of IL. In fact, in the case of CMImCl, only an equimolar amount of IL (with respect to WCl_6) led to the formation of nanorods, while increasing the IL amount led to irregular particles being formed. Using BMImCl (butyl group on the imidazolium

cation), the situation was the opposite: an equimolar amount of IL led to the formation of irregular particles, while an excess of IL yielded nanoparticle-constructed spheres.

The authors suggested that in the case of CMImCl, the IL can be selectively adsorbed on the surface of crystals, thus leading to an alteration of the anisotropic growth process. In the case of BMImCl, the hypothesis is that this IL can act as a template for the growth of nanospheres. The spheres, once formed, aggregate by different kind of interactions (electrostatic, hydrogen bonding, π-π stacking), yielding the nanoparticle-constructed spheres.

The produced WO_3 nanoparticles were used in conductimetric sensors for the detection of various pollutant gases (ethanol, methanol, isopropanol, ethyl acetate, toluene); the optimal temperature of the sensors was 240–300 °C, with short response (3–25 s, depending on the analyte and its concentration) and recovery times, and with 5 ppm as the lower detection limit.

Furthermore, Cheng and coworkers reported the use of an imidazolium IL (1-butyl-3-methylimidazolium tetrafluoroborate) in the process of WO_3 nanoparticle formation [117]. The nanoparticles were characterized using IR, XPS and XRD analyses. The produced nanoparticles were tested in a NO_2 electrochemical sensor, showing enhanced properties with respect to the corresponding WO_3 nanoparticles sensor in which no IL was used. The authors suggested that the better performances could be due to residue IL on the surface of the particles, with increased oxygen adsorption. The lower detection limit was 0.1 ppm, with a very high selectivity towards NO_2 (in the presence of ethanol, nitrobenzene, acetone, ammonia, carbon dioxide, etc) at the noteworthy low temperature of 50 °C. The reaction is the adsorption and reduction of NO_2 (outlined in Figure 4), which, in the presence of oxygen, yields NO_3^-, followed by the formation of a superoxide anion. This process traps electrons from WO_3 particles, leading to an increase of sensor resistance.

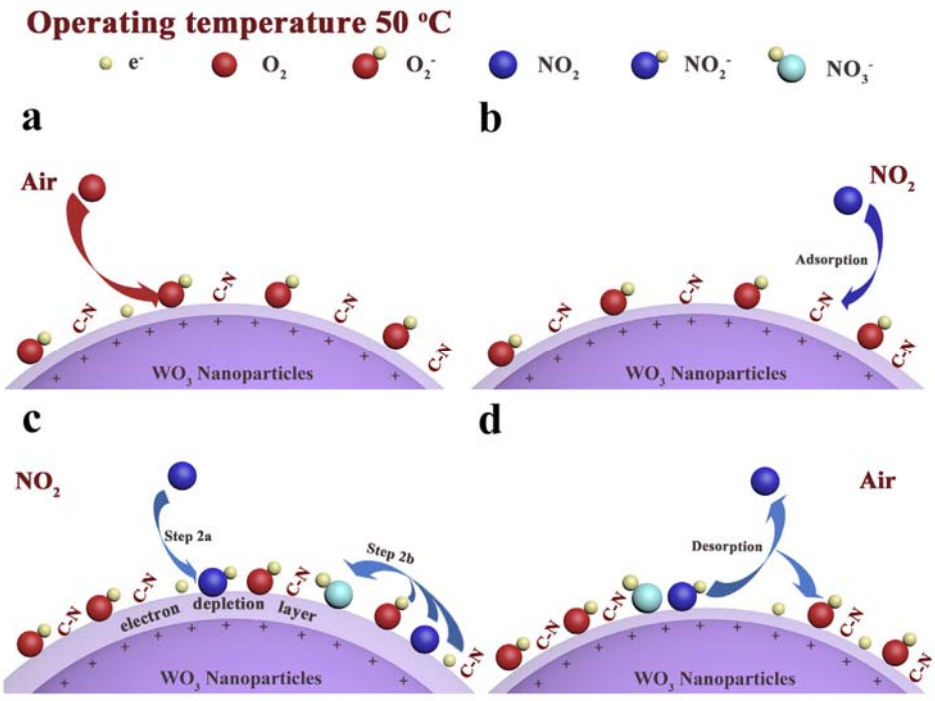

Figure 4. Proposed NO_2 detection mechanism. Reproduced with permission [117]. Copyright 2019, Elsevier.

As previously stated, outdoor gas detection suffers from high humidity levels, which in most cases lower the sensor performances. ILs can overcome (in part) this problem, as reported by Bendahan and coworkers, regarding a WO_3 sensor for aromatic volatile compounds (benzene, toluene, ethylbenzene and xylenes) [118]. A cheap and reliable removable filter, based on common imidazolium ILs,

was englobed into the sensor, with no loss in sensitivity and selectivity, for the efficient removal of most of the humidity, with significant improvement of the sensor performances, as reported in Figure 5.

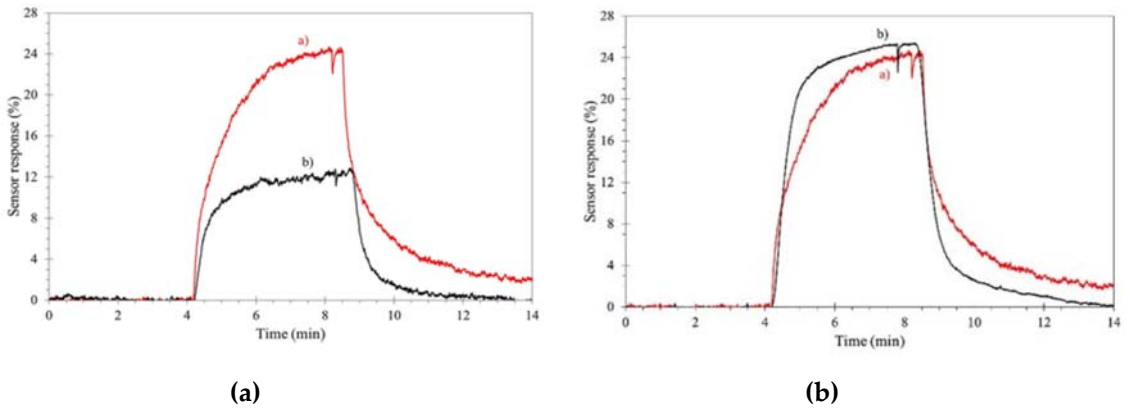

Figure 5. Effect of an ionic liquid (IL)-composed filter on aromatic volatile compound detection. Sensor response under 500 ppb compounds. (**a**): dry air; (**b**): wet (50%) air. Left, without filter, right with filter. Reproduced with permission [118]. Copyright 2018, ISFA.

Mahmoud and coworkers reported the use of WO_3 nanoparticles, obtained using a sol-gel method and glycerol IL, as components of a flexible poly-vinyl alcohol (PVA) membrane inserted between the two electrodes of a portable H_2S electrochemical sensor [119]. Along with excellent reproducibility of the results and long-term stability, the best operation temperature was quite low (80 °C), with a reasonable response time (19.1 ± 3.4 s). This result is quite significative, as the majority of metal oxide-based sensors operate at higher temperatures (200 °C or higher). The detection limit of this sensor was 10 ppm of H_2S, also in the presence of noteworthy amounts of interferents (H_2, C_2H_4), as reported in Figure 6.

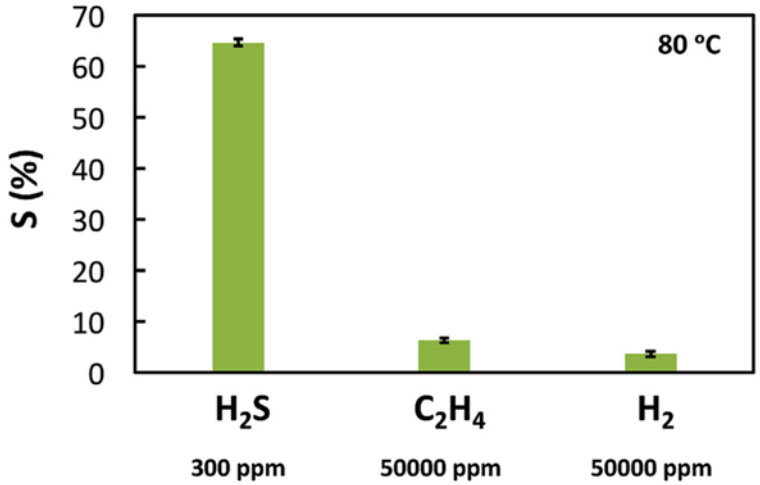

Figure 6. Selectivity of a WO_3 nanoparticles-glycerol IL-based H_2S sensor when exposed to H_2S, H_2 and C_2H_4 at 80 °C. Reproduced with permission [119]. Copyright 2017, Elsevier.

This electrochemical sensor is based on electrochemical reduction of H_2S in the presence of adsorbed oxygen, generating SO_2. The same authors reported an improvement of the H_2S sensor using chitosan instead of poly-vinyl alcohol (PVA) in the flexible membrane (containing WO_3 nanoparticles and IL), obtaining an electrochemical sensor less humidity dependent and working at the very low temperature of 40 °C [84]. In this case, the cooperation of WO_3 nanoparticles, adsorbed oxygen, IL and chitosan seems to allow better results, as depicted in Figure 7.

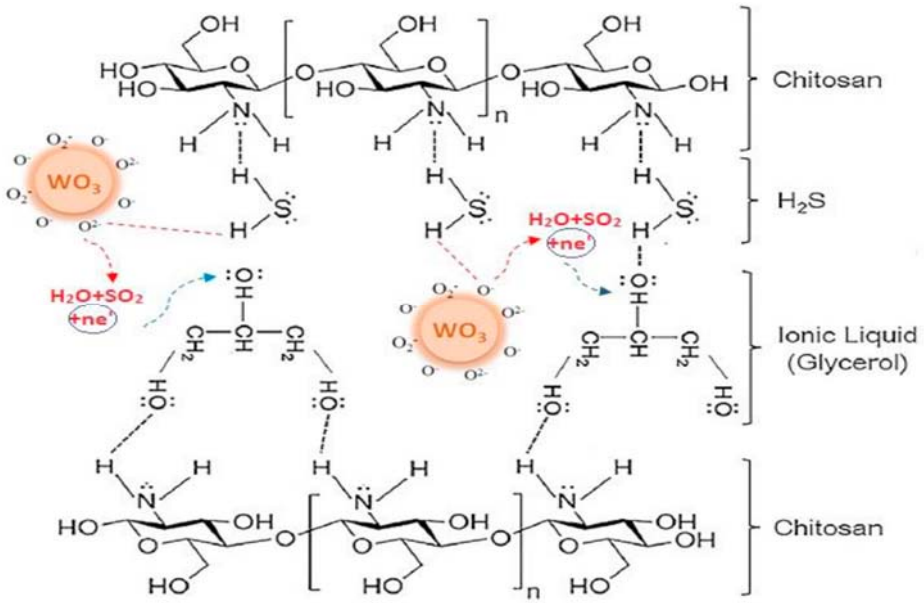

Figure 7. Participation of all sensor components in H_2S detection at 40 °C. Reproduced with permission [84]. Copyright 2020, Elsevier.

The possibility of using a common imidazolium IL (EMIm-BF_4) in a conductimetric CO_2 gas sensor was recently reported by Daves and Ersoez [120]. In particular, the authors exploited the properties of organic IL, while combining them with the mechanical stability of inorganic compounds. The electrochemical sensor was formed using an ionogel (obtained by the combination of the IL and an inorganic porous host) deposited over WO_3. The very good performances of this kind of sensor are due to the permeability to CO_2 of the ionogel layer (also compared to pure IL, due to the high enhancement of the surface for the presence of the porous inorganic host).

Although ILs have only recently started to be used to enhance the performances of metal oxide-based electrochemical gas sensors (with reference, in particular, to WO_3-based sensors), the recognition of their role has been clearly asserted. In fact, not only ILs do heavily influence the structure of WO_3 nanoparticles when used in the synthetic step (nanoplates, nanorods, nanospheres, etc.), but their residues, eventually present on the surface of nanoparticles, can improve the sensed gas adsorption, thus yielding better performances. We hope that the virtually infinite possibility to vary the structures of ILs (and thus their physico-chemical characteristics) will lead to the fabrication of organic-inorganic hybrid devices with optimal gas sensing performances, in terms of sensitivity, selectivity, reproducibility and low humidity dependence.

3. WO_3 and Ionic Liquids in Fuel Desulfurization

One of the main problems in fuel combustion (beside CO_2 formation) is the production of polluting and toxic gases, such as SO_2 and SO_3. In particular, naphtha shows the highest sulfur and olefine content, with a high octane number. The target of the desulfurization process is thus the elimination of the highest possible sulfur amount, while preserving a high olefine content (maintaining a high octane rating), in order to have good fuel performances during combustion, lowering to a minimum level the emissions of sulfurated compounds.

Of the organic sulfur compounds present in petroleum derivatives, thiols, sulfides, disulfides and thiophenes are among the most important (Figure 8).

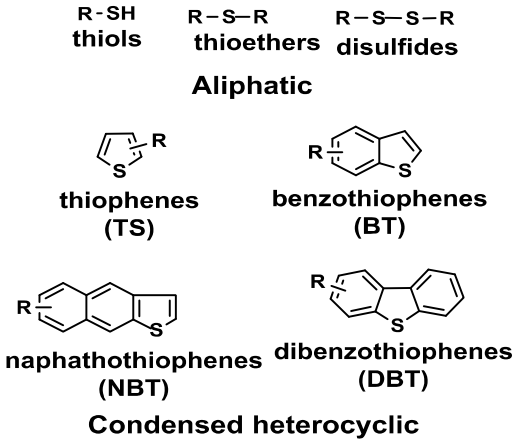

Figure 8. Main sulfur-containing compounds in petroleum fuels. Reproduced with permission [121]. Copyright 2016, Elsevier.

Regarding the available methods to carry out liquid fuel desulfurization, hydrodesulfurization (HDS) and oxidative desulfurization (ODS) are among the most used.

3.1. WO_3 and Ionic Liquids in Hydrodesulfurization (HDS)

Hydrodesulfurization (HDS) is the removal of sulfur compounds from liquid petroleum derivatives by reaction with molecular hydrogen at a high temperature (300–350 °C). High pressures of H_2 are needed for this reaction (20–100 atm), and sulfur compounds are transformed into H_2S and hydrocarbons in the presence of catalysts. H_2S is at the end removed from the reaction mixture and transformed into elemental sulfur [121]. This process is quite efficient to remove aliphatic compounds (thiols, sulfides, disulfides), while thiophene derivatives are quite recalcitrant, needing more drastic conditions, which influence the cost of the process, among other things. The difficulty of removing thiophenes seems to be related to a lower adsorption on the catalyst surface.

ILs can play an important role in catalyst synthesis, in order to obtain compounds with improved performances. To this regard, it should be remembered that HDS catalysts promote both sulfur transformation into H_2S and olefine saturation, which is a highly undesired side reaction (lowering the octane number of the produced fuel). Daage and Chianelli [122] and Topsøe [123] elaborated a model to understand the selectivity of desulfuration over olefine saturation using supported metal sulfide catalysts (the brim-edge model). In particular, the brim sites of a multistack metal sulfide HDS catalyst (the top and bottom layers) catalyze both hydrodesulfuration and olefine saturation, while the edge sites catalyze only hydrodesulfuration. The conclusion is that a good HDS catalyst contains a high edge to brim ratio, and this ratio can be in part controlled by controlling the interactions between the catalyst and its support (necessary to disperse the metal catalyst, enhancing its surface). Such an interaction should be a compromise in order to have good metal dispersion, minimizing side reactions. Moreover, the incorporation of a "promoting element" (usually Co or Ni) can increase the number of edge sites.

Bao, Yuan and coworkers reported that the use of an IL, tetraethylammonium bromide (TEAB), in an aqueous solution at room temperature allowed an organic-inorganic nanocomposite ($TEA_2W_6O_{19}$) to be formed [124]. The characteristic of such a composite was its core-shell structure ($W_6O_{19}{}^{=}$ core and TEA^+ shell), which led to monodispersion, useful to deposit it onto alumina (the support) in the presence of a Ni promoter. The amount of dispersed Ni, along with the kind of dispersion, created catalyst structures with different edge to brim ratios, as evidenced in Figure 9. For a useful comparison, a catalyst obtained using the conventional impregnation method is also reported (Figure 9d).

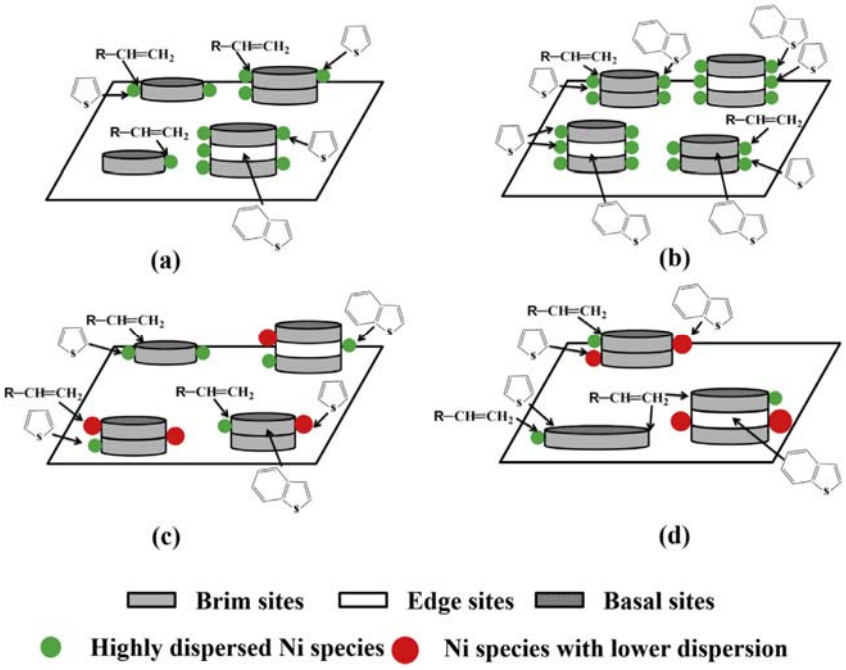

Figure 9. Schematic representation of different supported Ni promoted WO_3/Al_2O_3 catalysts. NiO content: (**a**) < 4.8 wt.%, (**b**) 4.8 wt.%, (**c**) > 4.8 wt.%, (**d**) 4.8 wt.% (impregnation method). Reproduced with permission [124]. Copyright 2015, Elsevier.

The catalysts thus obtained, with a compromise between metal dispersion and stacking, yielded enhanced performances, of which the improvement of HDS selectivity, minimizing olefine saturation, was of noteworthy importance. The ability of ILs to induce the formation of particular structures (in this case a core-shell one) allowed the improvement of the catalyst performances.

3.2. WO_3 and Ionic Liquids in Oxidative Desulfurization (ODS)

As previously said, thiophene derivatives are less prone to HDS reaction. In order to improve thiophenes abatement, while maintaining acceptable process costs, oxidative desulfurization (ODS) can be considered a promising method, due to its simplicity and high efficiency [121,125,126]. ODS is the chemical oxidation of sulfur compounds in liquid fuels (using as an example H_2O_2 as oxidant), yielding products which can be easily removed from the reaction mixture using a non-miscible solvent. In this regard, ILs can be efficiently used as extractive solvents of both starting and oxidized sulfur compounds and can be considered "greener" alternatives to conventional volatile organic compounds (VOCs).

As an example, Li and coworkers efficiently carried out the oxidative desulfurization of fuel using H_2O_2 as the oxidant agent in the presence of a WO_3/C composite catalyst [127]. The extraction of sulfur compounds was carried out using an imidazolium IL (1-ethyl-3-methylimidazolium ethyl sulfate), added to the fuel as a non-miscible solvent (biphasic reaction medium). The WO_3/C composite was oxidized to the complex $H_2[W_2O_3(O_2)_4(H_2O)_2]_2$ in the IL phase, which also extracted from fuel the aromatic sulfur compounds; the complex then oxidized dibenzothiophene (DBT) to its sulfone ($DBTO_2$), which remained in the IL phase, allowing an easy separation. The same process could be carried out using 1-butyl-3-methylimidazolium tetrafluoroborate as $DBTO_2$ extraction solvent [128].

In addition, Zhu, Li and coworkers reported the ability of an imidazolium IL (C_{16}MImBr) to direct the synthesis of a WO_3-SiO_2 composite towards a mesoporous material (W-SiO_2-20, Figure 10), which exhibited a high dispersion of tungsten throughout the structure (enhancing the catalytic activity) [129]. The synthesis of the mesoporous catalyst was carried out starting from a polyoxometalate compound ($[C_{16}mim]_3PW_{12}O_{40}$) in a one-pot gel of tetraethyl orthosilicate, which was then calcinated at 550 °C.

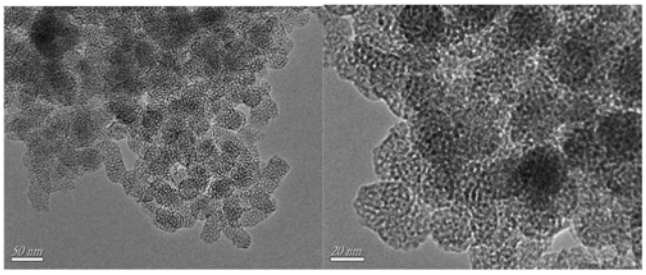

Figure 10. TEM images of the W-SiO_2-20 catalyst. Reproduced with permission [129]. Copyright 2016, Elsevier.

The mesoporous catalyst was characterized using the usual techniques and efficiently used in ODS reactions (Figure 11) at the low temperature of 60 °C. The reaction times were quite short and very good yields were obtained after only 30 min. Moreover, the process did not require additional organic solvents as extractants.

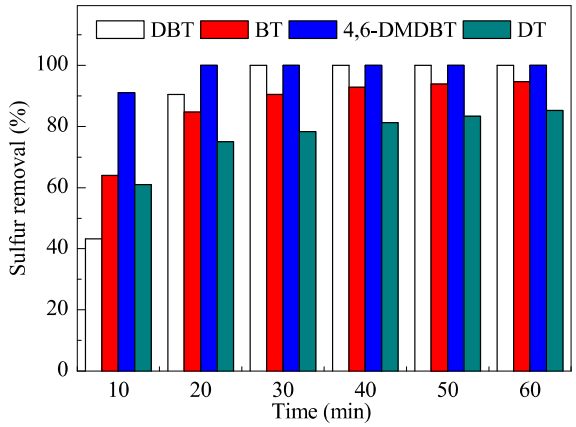

Figure 11. Removal of sulfur compounds in oxidative desulfurization (ODS) with the W-SiO_2-20 catalyst. DBT: dibenzothiophene; BT: benzothiophene; 4,6-DMDBT: 4,6-dimethyldibenzothiophene; DT: 1-dodecanethiol. Reproduced with permission [129]. Copyrights 2016, Elsevier.

The same authors reported a similar synthesis, utilizing a different support (in this case mesoporous ZrO_2) evidencing as both IL and calcination temperature, influenced the morphology and the dispersion of WO_3 [130]. The best obtained catalyst (calcinated at 700 °C, using a C_{16}-ammonium IL, 700-C_{16}-WO_3/ZrO_2) performed very well in oxidation desulfurization. Dibenzothiophene (DBT) could be completely oxidized to DBT sulfone (DBTO2). Moreover, the catalyst could be recycled ten times with very low efficiency loss.

A functional IL ($[(C_{16}H_{33})_2N(CH_3)_2]_2W_2O_{11}$) acted as WO_3 nanoparticle precursor and a large surface area (203 m^2/g) few-layer g-C_3N_4 support was used to disperse them, yielding a supported catalyst [131]; this composite was characterized using SEM (Figure 12), TEM, FT-IR, XRD and XPS, showing highly dispersed nanoparticles. The analysis showed that during the synthetic process of WO_3 dispersion on the support, the structure of few-layer g-C_3N_4 was not destroyed (Figure 12D vs C), leading to a WO_3 catalyst with a very high surface, not obtainable using pure WO_3, whose structure showed agglomerates (Figure 12A).

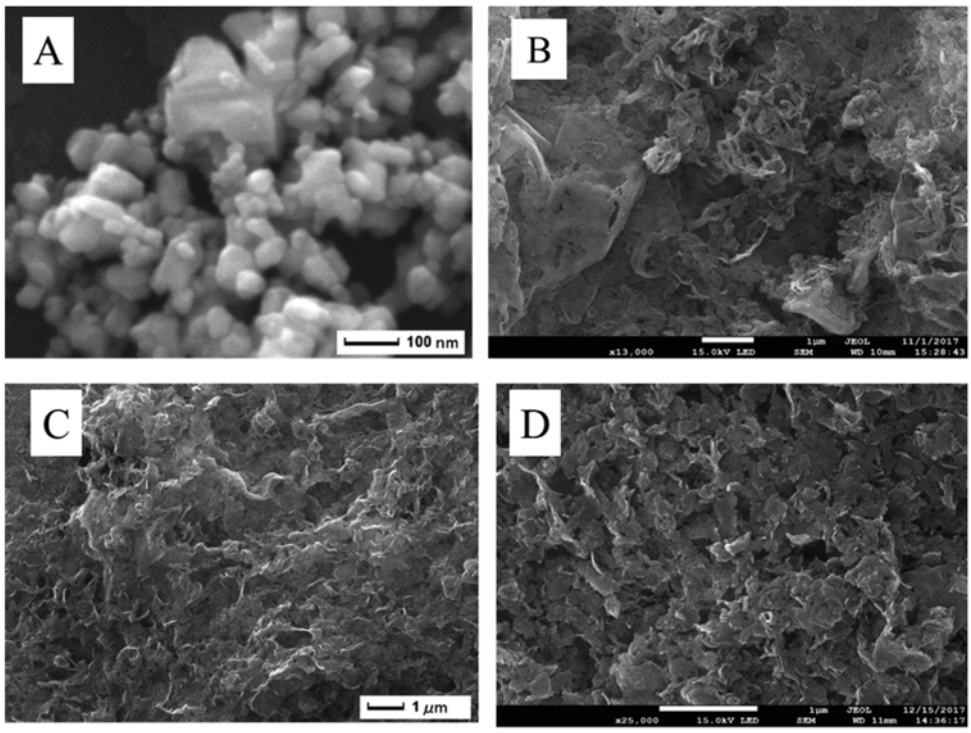

Figure 12. SEM images of (**A**) WO_3, (**B**) bulk g-C_3N_4, (**C**) few-layer g-C_3N_4, (**D**) WO_3/few-layer g-C_3N_4. Reproduced with permission [131]. Copyright 2019, Elsevier.

The enormous amount of exposed active sites rendered the composite an excellent catalyst in ODS processes, with the removal of 100% refractory sulfur-containing molecules at 50 °C in 1 h. Moreover, the catalyst was recycled up to six times without efficiency loss. A possible reaction mechanism is depicted in Figure 13.

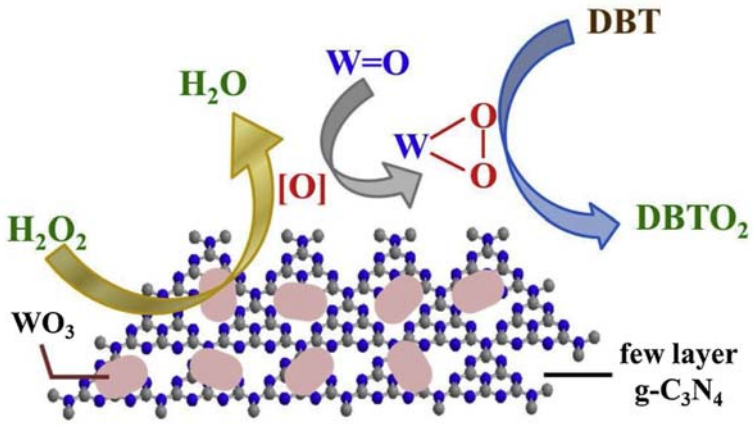

Figure 13. Possible ODS mechanism using WO_3/few-layer g-C_3N_4 as catalyst. Reproduced with permission [131]. Copyright 2019, Elsevier.

Last, tungsten trioxide-carbon nanotubes composite (WO_3/CNT) was demonstrated to be a very good catalyst in ODS of recalcitrant aromatic sulfur compounds, as reported by Li and coworkers [132]. The catalyst synthesis was quite easy and was carried out in the presence of an imidazolium IL (C_{16}MImCl), using phosphotungstic acid (HPW) as tungsten source (Figure 14).

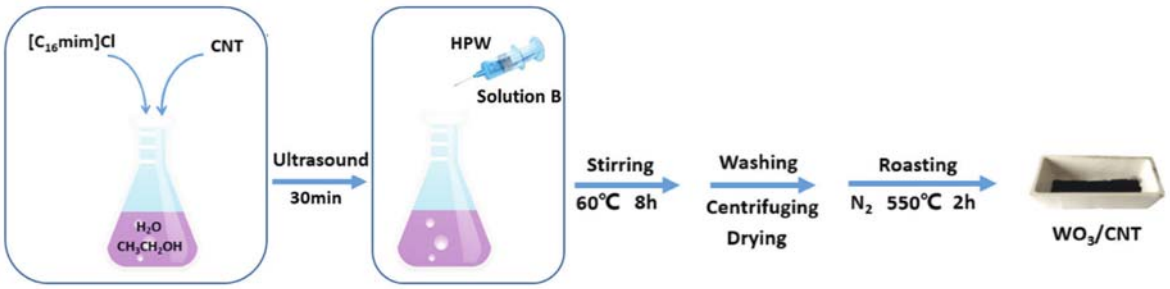

Figure 14. Schematic description of WO_3/CNT catalyst preparation. Reproduced with permission [132]. Copyright 2019, Wiley and Society of Chemical Industry.

The characterization of such a composite showed that the IL played a crucial role in determining the dispersion degree and the crystal phase of WO_3 on the carrier (carbon nanotube, CNT). In fact, the IL improved the transformation of tungsten trioxide from monoclinic to tetragonal, inhibiting at the same time the growth of metal oxide grains. In this way, high WO_3 dispersion was obtained, enhancing the catalytic activity. Moreover, a comparison of catalytic activity of different supported tungsten oxide forms was carried out, demonstrating the following activity order in sulfur oxidative removal: tetrahedral > tetragonal > monoclinic.

In conclusion, this section demonstrated the possibility of using an IL to enhance WO_3 dispersion on an inorganic support, ensuring the formation of composites with a very large number of exposed catalytic sites. In addition, in some cases the IL was demonstrated to be able to direct the morphology of WO_3 particles.

4. Conclusions and Perspectives

The synergy between WO_3 and ILs in increasing the performances of the corresponding devices is quite recent. During the last decade, ILs were demonstrated to be able to enhance the ability of tungsten trioxide in polluting gas sensing and in desulfurization processes, and the increasing number of publications on this topic gives an idea of future developments. This is due to the virtually infinite possibility to vary the structures of ILs (and thus their physico-chemical characteristics) changing the nature of cation and anion.

As ILs interact well with metal oxides (in particular with WO_3), they can be easily used as alternatives to classical organic solvents, with the advantage of minimizing air pollution (due to their virtually null vapor pressure) and the actual possibility of their recycling. Moreover, their ability to dissolve inorganic compounds can play a noteworthy role in producing highly dispersed composites, enhancing their activity. Furthermore, their hygroscopy can be successfully exploited in producing gas sensors with increased resistance to high humidity levels (especially for outdoor devices, for which humidity can be a serious problem). When using an IL in WO_3 production processes, it is possible to induce the formation of particular structures (nanorods, nanospheres, etc.), depending on the nature of the IL. Moreover, in some cases these salts are inglobated into the metal oxide structure, enhancing the performances of the corresponding gas sensor by increasing the gas adsorption on the surface of the composite.

It is thus probable that in the near future these peculiarities of ILs will lead to devices with better sensing performances, also lowering the environmental impact by choosing biocompatible ILs.

Another approach to air pollutants, besides their sensing and removal, is related to the decrease of their production. In particular, when referring to outdoor air pollution, fuel combustion plays a giant part. It is thus important to remove any possible source of pollution before combustion, in order to lower the environmental impact. As sulfur oxides are among the toxic pollutants deriving from fuel combustion, fuel desulfurization is a priority for the oil industry.

In this context, WO_3 in combination with ILs plays a pivotal role. In fact, ILs enhance the extent of adsorption of sulfur derivatives on the surface of the WO_3 catalyst, enabling better conversions also in the case of thiophene derivatives, which are among the most refractory sulfur compounds in fuel.

Although it is not possible, at this stage, to define the optimal WO_3 nanostructure morphology for all the applications reported in this review, the strong suggestion evinced from literature data is the ability of ILs to induce the formation of core-shell nanostructures allowing the improvement of the catalyst performances. The higher the surface to volume ratio, the better the performances of the WO_3 catalyst, both in the case of pure tungsten oxide compounds (higher number of active sites), and in the case in which IL fragments are present on the catalyst surface (allowing for a higher number of functionalized sites). Moreover, nanoparticles of 10-50 nm size seem optimal for the applications here reported.

Due to the increasing work of the scientific community in producing task-specific ILs showing better performances, along with an environmentally benign fingerprint (from both synthetic and disposal point of view, using biomasses as starting materials), we are confident that the synergy between ILs and metal oxides will make a considerable contribution to the field of air pollutant sensing and remediation.

Author Contributions: All authors contributed equally to this manuscript. All authors have read and agreed to the published version of the manuscript.

Funding: This research was funded by the University of Palermo and by Sapienza University of Rome, grant number RM11916B462FA71F.

Acknowledgments: The authors want to thank Marco Di Pilato for technical support.

Conflicts of Interest: The authors declare no conflict of interest. The funders had no role in the design of the study; in the collection, analyses, or interpretation of data; in the writing of the manuscript, or in the decision to publish the results.

References

1. Kwong, W.L.; Savvides, N.; Sorrell, C.C. Electrodeposited nanostructured WO_3 thin films for photoelectrochemical applications. *Electrochim. Acta* **2012**, *75*, 371–380. [CrossRef]
2. Yu, J.; Qi, L. Template-free fabrication of hierarchically flower-like tungsten trioxide assemblies with enhanced visible-light-driven photocatalytic activity. *J. Hazard. Mater.* **2009**, *169*, 221–227. [CrossRef] [PubMed]
3. Amano, F.; Ishinaga, E.; Yamakata, A. Effect of Particle Size on the Photocatalytic Activity of WO_3 Particles for Water Oxidation. *J. Phys. Chem. C* **2013**, *117*, 22584–22590. [CrossRef]
4. Long, H.; Zeng, W.; Zhang, H. Synthesis of WO_3 and its gas sensing: A review. *J. Mater. Sci.: Mater. Electron.* **2015**, *26*, 4698–4707. [CrossRef]
5. Grilli, M.L.; Chevallier, L.; Vona, M.L.D.; Licoccia, S.; Bartolomeo, E.D. Planar electrochemical sensors based on YSZ with WO_3 electrode prepared by different chemical routes. *Sensors Actuator. B Chem.* **2005**, *111*, 91–95. [CrossRef]
6. Lu, R.; Zhong, X.; Shang, S.; Wang, S.; Tang, M. Effects of sintering temperature on sensing properties of WO_3 and Ag-WO_3 electrode for NO_2 sensor. *R. Soc. Open Sci.* **2018**, *5*, 171691. [CrossRef] [PubMed]
7. Dutta, A.; Kaabbuathong, N.; Grilli, M.L.; Di Bartolomeo, E.; Traversa, E. Study of YSZ-Based Electrochemical Sensors with WO_3 Electrodes in NO_2 and CO Environments. *J. Electrochem. Soc.* **2003**, *150*, H33–H37. [CrossRef]
8. Yamazoe, N. New approaches for improving semiconductor gas sensors. *Sens. Actuators B Chem.* **1991**, *5*, 7–19. [CrossRef]
9. Granqvist, C.G. Electrochromic tungsten oxide films: Review of progress 1993–1998. *Sol. Energy Mater. Sol. Cells* **2000**, *60*, 201–262. [CrossRef]
10. Masetti, E.; Grilli, M.L.; Dautzenberg, G.; Macrelli, G.; Adamik, M. Analysis of the influence of the gas pressure during the deposition of electrochromic WO_3 films by reactive r.f. sputtering of W and WO_3 target. *Solar Energy Mater. Solar Cells* **1999**, *56*, 259–269. [CrossRef]
11. Rao, M.C. Structure and properties of WO_3 thin films for electrochromic device application. *J. Non-Oxide Glasses* **2013**, *5*, 1–8.

12. Arvizu, M.A.; Qu, H.-Y.; Cindemir, U.; Qiu, Z.; Rojas-González, E.A.; Primetzhofer, D.; Granqvist, C.G.; Österlund, L.; Niklasson, G.A. Electrochromic WO_3 thin films attain unprecedented durability by potentiostatic pretreatment. *J. Mater. Chem. A* **2019**, *7*, 2908–2918. [CrossRef] [PubMed]
13. Tang, C.-J.; He, J.-L.; Jaing, C.-C.; Liang, C.-J.; Chou, C.-H.; Han, C.-Y.; Tien, C.-L. An All-Solid-State Electrochromic Device Based on WO_3–Nb_2O_5 Composite Films Prepared by Fast-Alternating Bipolar-Pulsed Reactive Magnetron Sputtering. *Coatings* **2019**, *9*, 9. [CrossRef]
14. Valerini, D.; Hernández, S.; Di Benedetto, F.; Russo, N.; Saracco, G.; Rizzo, A. Sputtered WO_3 films for water splitting applications. *Mater. Sci. Semicon. Proc.* **2016**, *42*, 150–154. [CrossRef]
15. Gerand, B.; Nowogrocki, G.; Guenot, J.; Figlarz, M. Structural study of a new hexagonal form of tungsten trioxide. *J. Solid State Chem.* **1979**, *29*, 429–434. [CrossRef]
16. Sun, W.; Yeung, M.T.; Lech, A.T.; Lin, C.-W.; Lee, C.; Li, T.; Duan, X.; Zhou, J.; Kaner, R.B. High surface area tunnels in hexagonal WO_3. *Nano Lett.* **2015**, *15*, 4834–4838. [CrossRef]
17. Lee, T.; Lee, Y.; Jang, W.; Soon, A. Understanding the advantage of hexagonal WO_3 as an efficient photoanode for solar water splitting: A first-principles perspective. *J. Mater. Chem. A* **2016**, *4*, 11498–11506. [CrossRef]
18. Kollender, J.P.; Gallistl, B.; Mardare, A.I.; Hassel, A.W. Photoelectrochemical water splitting in a tungsten oxide—nickel oxide thin film material library. *Electrochim. Acta* **2014**, *140*, 275–281. [CrossRef]
19. Wiseman, P.J.; Dickens, P.G. The crystal structure of cubic hydrogen tungsten bronze. *J. Solid State Chem.* **1973**, *6*, 374–377. [CrossRef]
20. Mardare, C.C.; Hassel, A.W. Review on the Versatility of Tungsten Oxide Coatings. *Phys. Status Solidi A* **2019**, *216*, 1900047. [CrossRef]
21. Biswas, S.K.; Baeg, J.O. A facile one-step synthesis of single crystalline hierarchical WO_3 with enhanced activity for photoelectrochemical solar water oxidation. *Int. J. Hydrog. Energy* **2013**, *8*, 3177–3188. [CrossRef]
22. Gullapalli, S.K.; Vemuri, R.S.; Ramana, C.V. Structural transformation induced changes in the optical properties of nanocrystalline tungsten oxide thin films. *Appl. Phys. Lett.* **2010**, *96*, 171903. [CrossRef]
23. Inoue, T.; Ohtsuka, K.; Yoshida, Y.; Matsuura, Y.; Kajiyama, Y. Metal oxide semiconductor NO_2 sensor. *Sens. Actuators B* **1995**, *25*, 388–391. [CrossRef]
24. Kim, T.; Kim, Y.; Yoo, K.S.; Sung, G.; Jung, H. Sensing characteristics of dc reactive sputtered WO_3 thin films as an NO_x gas sensor. *Sens. Actuators B Chem.* **2000**, *62*, 102–108. [CrossRef]
25. Qin, Y.X.; Ye, Z.H. DFT study on interaction of NO_2 with the vacancy-defected WO_3 nanowires for gas-sensing. *Sens. Actuators B Chem.* **2016**, *222*, 499–507. [CrossRef]
26. Di Bartolomeo, E.; Grilli, M.L.; Yoon, J.W.; Traversa, E. Zirconia-Based Electrochemical NO_x Sensors with Semiconducting Oxide Electrodes. *J. Am. Ceram. Soc.* **2004**, *87*, 1883–1889. [CrossRef]
27. Di Bartolomeo, E.; Grilli, M.L.; Traversa, E. Sensing Mechanism of Potentiometric Gas Sensors Based on Stabilized Zirconia with Oxide Electrodes, Is It Always Mixed Potential? *J. Electrochem. Soc.* **2004**, *151*, H133–H139. [CrossRef]
28. Maekawa, T.; Tamaki, J.; Miura, N.; Yamazoe, N. Gold-loaded tungsten-oxide sensor for detection of ammonia in air. *Chem. Lett.* **1992**, *4*, 639–642. [CrossRef]
29. Meixner, H.; Gerblinger, J.; Lampe, U.; Fleischer, M. Thin-film gas sensors based on semiconducting metal oxides. *Sens. Actuators B* **1995**, *23*, 119–125. [CrossRef]
30. Ruokamo, I.; Karkkainen, T.; Huusko, J.; Ruokanen, T.; Blomberg, M.; Torvela, H.; Lantto, V. H_2S response of WO_3 thin film sensors manufactured by Silican processing technology. *Sens. Actuators B* **1994**, *19*, 486–488. [CrossRef]
31. Zhu, L.F.; She, J.C.; Luo, J.Y.; Deng, S.Z.; Chen, J.; Xu, N.S. Study of Physical and Chemical Processes of H_2 Sensing of Pt-Coated WO_3 Nanowire Films. *Phys. Chem. C* **2010**, *114*, 15504–15509. [CrossRef]
32. Shimizu, Y.; Matsunaga, N.; Hyodo, T.; Egashira, M. Improvement of SO_2 Sensing Properties of WO_3 by Noble Metal Loading. *Sens. Actuators B Chem.* **2011**, *77*, 35–40. [CrossRef]
33. Grilli, M.L.; Di Bartolomeo, E.; Lunardi, A.; Chevallier, L.; Cordiner, S.; Traversa, E. Planar non-nernstian electrochemical sensors: Field test in the exhaust of a spark ignition engine. *Sens. Actuators B Chem.* **2005**, *108*, 319–332. [CrossRef]
34. Grilli, M.L.; Kaabbuathong, N.; Dutta, A.; Di Bartolomeo, E.; Traversa, E. Electrochemical NO_2 sensors with WO_3 electrodes for high temperature applications. *J. Ceramic Soc. Jpn.* **2002**, *110*, 159–162. [CrossRef]
35. Yamazoe, N.; Shimanoe, K. Theory of Power Laws for Semiconductor Gas Sensors. *Sens. Actuators B Chem.* **2008**, *128*, 566–573. [CrossRef]

36. Wang, C.; Yin, L.; Zhang, L.; Xiang, D.; Gao, R. Metal Oxide Gas Sensors: Sensitivity and Influencing Factors. *Sensors* **2010**, *10*, 2088–2106. [CrossRef]
37. Xu, C.; Tamaki, J.; Miura, N.; Yamazoe, N. Grain size effects on gas sensitivity of porous SnO_2-based elements. *Sens. Actuators B* **1991**, *3*, 147–155. [CrossRef]
38. Lin, T.; Lv, X.; Li, S.; Wang, Q. The Morphologies of the Semiconductor Oxides and Their Gas-Sensing Properties. *Sensors* **2017**, *17*, 2779. [CrossRef]
39. Li, X.L.; Lou, T.J.; Sun, X.M.; Li, Y.D. Highly sensitive WO_3 hollow-sphere gas sensors. *Inorg. Chem.* **2004**, *43*, 5442–5449. [CrossRef]
40. Yao, Y.; Ji, F.; Yin, M.; Ren, X.; Ma, Q.; Yan, J.; Liu, S.F. Ag Nanoparticle-sensitized WO_3 hollow nanosphere for localized surface plasmon enhanced gas sensors. *ACS Appl. Mat. Interface.* **2016**, *8*, 18165–18172. [CrossRef]
41. Kong, W.; Zhang, R.; Zhang, X.; Ji, L.; Yu, G.; Wang, T.; Luo, Y.; Shi, X.; Xu, Y.; Sun, X. WO_3 nanosheets rich in oxygen vacancies for enhanced electrocatalytic N_2 reduction to NH_3. *Nanoscale* **2019**, *11*, 19274–19277. [CrossRef] [PubMed]
42. Liu, Z.; Miyauchi, M.; Yamazaki, T.; Shen, Y. Facile synthesis and NO_2 gas sensing of tungsten oxide nanorods assembled microspheres. *Sens. Actuators B* **2009**, *140*, 514–519. [CrossRef]
43. Cao, B.; Chen, J.; Tang, X.; Zhou, W. Growth of monoclinic WO_3 nanowire array for highly sensitive NO_2 detection. *J. Mater. Chem.* **2009**, *19*, 2323–2327. [CrossRef]
44. Cai, Z.-X.; Li, H.-Y.; Yang, X.-N.; Guo, X. NO sensing by single crystalline WO_3 nanowires. *Sens. Actuators B* **2015**, *219*, 346–353. [CrossRef]
45. Ji, H.; Zeng, W.; Li, Y. Gas sensing mechanisms of metal oxide semiconductors: A focus review. *Nanoscale* **2019**, *11*, 22664–22684. [CrossRef]
46. Yan, H.; Zhang, X.; Zhou, S.; Xie, X.; Luo, Y.; Yu, Y. Synthesis of WO_3 nanoparticles for photocatalytic O_2 evolution by thermal decomposition of ammonium tungstate loading on g-C3N4. *J. Alloys Compounds* **2011**, *509*, L232–L235. [CrossRef]
47. Gomez, C.; Sánchez Martínez, D.; Juarez, I.; Martinez, A.; Torres-Martínez, L. Facile synthesis of m-WO_3 powders via precipitation in ethanol solution and evaluation of their photocatalytic activities. *J. Photochem. Photobiol. A: Chem.* **2013**, *262*, 28–33. [CrossRef]
48. Kondalkar, V.V.; Kharade, R.R.; Mali, S.S.; Mane, R.M.; Patil, P.B.; Patil, P.S.; Choudhury, S.; Bhosale, P.N. Nanobrick-like WO_3 thin films: Hydrothermalsynthesis and electrochromic application. *Superlattices Microstruct.* **2014**, *73*, 290–295. [CrossRef]
49. Kida, T.; Nishiyama, A.; Hua, Z.; Suematsu, K.; Yuasa, M.; Shimanoe, K. WO_3 nanolamella gas sensor: Porosity control using SnO_2 nanoparticles for enhanced NO_2 sensing. *Langmuir* **2014**, *30*, 2571–2579. [CrossRef]
50. Meng, Z.; Fujii, A.; Hashishin, T.; Wada, N.; Sanada, T.; Tamaki, J.; Kojima, K.; Haneoka, h.; Suzuki, T. Morphological and crystal structural control of tungsten trioxide for highly sensitive NO_2 gas sensors. *J. Mater. Chem. C* **2015**, *3*, 1134–1141. [CrossRef]
51. Meulenkamp, E.A. Mechanism of WO_3 Electrodeposition from Peroxy-Tungstate Solution. *J. Electrochem. Soc.* **1997**, *144*, 1664–1671. [CrossRef]
52. Breedon, M.; Spizzirri, P.; Taylor, M.; du Plessis, J.; McCulloch, D.; Zhu, J.; Yu, L.; Hu, Z.; Rix, C.; Wlodarski, W.; et al. Synthesis of Nanostructured Tungsten Oxide Thin Films: A Simple, Controllable, Inexpensive, Aqueous Sol−Gel Method. *Cryst. Growth Des.* **2010**, *10*, 430–439. [CrossRef]
53. Yamada, Y.; Tabata, K.; Yashima, T. The character of WO_3 film prepared with RF sputtering. *Solar Ener. Mater. Solar Cells* **2007**, *91*, 29–37. [CrossRef]
54. Boyadjiev, S.I.; Georgieva, V.; Stefan, N.; Stan, G.E.; Mihailescu, N.; Visan, A.; Mihailescu, I.N.; Besleaga, C.; Szilágyi, I.M. Characterization of PLD grown WO_3 thin films for gas sensing. *Appl. Surf. Sci.* **2017**, *417*, 218–223. [CrossRef]
55. Li, S.; Yao, Z.; Zhou, J.; Zhang, R.; Shen, H. Fabrication and characterization of WO_3 thin films on silicon surface by thermal evaporation. *Mater. Lett.* **2017**, *195*, 213–216. [CrossRef]
56. Wang, C.-M.; Wen, C.-Y.; Chen, Y.-C.; Kao, K.-S.; Cheng, D.-L.; Peng, C.-H. Effect of Deposition Temperature on the Electrochromic Properties of Electron Beam-Evaporated WO_3 Thin Films. *Integr. Ferroelectr.* **2014**, *158*, 62–68. [CrossRef]

57. Blackman, I.C.S.; Parkin, P. Atmospheric Pressure Chemical Vapor Deposition of Crystalline Monoclinic WO_3 and WO_{3-x} Thin Films from Reaction of WCl_6 with O-Containing Solvents and Their Photochromic and Electrochromic Properties. *Chem. Mater.* **2005**, *17*, 1583–1590. [CrossRef]
58. Rogers, R.; Seddon, K.; Volkov, S. *Green Industrial Applications of Ionic Liquids*; Springer: Berlin/Heidelberg, Germany, 2002; Volume 818.
59. Holbrey, J.D.; Rogers, R.D. *Ionic Liquids in Synthesis*; Wasserscheid, P., Welton, T., Eds.; Wiley-VCH: Weinheim, Germany, 2008; Volume 1, pp. 57–174.
60. Wang, B.; Qin, L.; Mu, T.; Xue, Z.; Gao, G. Are ionic liquids chemically stable? *Chem. Rev.* **2017**, *117*, 7113–7131. [CrossRef]
61. Mahmood, H.; Moniruzzaman, M. Recent Advances of Using Ionic Liquids for Biopolymer Extraction and Processing. *Biotechnol. J.* **2019**, *14*, 1900072. [CrossRef]
62. Verma, C.; Mishra, A.; Chauhan, S.; Verma, P.; Srivastava, V.; Quraishi, M.A.; Ebenso, E.E. Dissolution of cellulose in ionic liquids and their mixed cosolvents: A review. *Sus. Chem. Pharm.* **2019**, *13*, 100162. [CrossRef]
63. Fang, Y.; Ma, P.; Cheng, H.; Tan, G.; Wu, J.; Zheng, J.; Zhou, X.; Fang, S.; Dai, Y.; Lin, Y. Synthesis of Low-Viscosity Ionic Liquids for Application in Dye-Sensitized Solar Cells. *Chem. Asian J.* **2019**, *14*, 4201–4206. [CrossRef] [PubMed]
64. Lobregas, M.O.S.; Camacho, D.H. Gel polymer electrolyte system based on starch grafted with ionic liquid: Synthesis, characterization and its application in dye-sensitized solar cell. *Electrochim. Acta* **2019**, *298*, 219–228. [CrossRef]
65. Dai, C.; Zhang, J.; Huang, C.; Lei, Z. Ionic Liquids in Selective Oxidation: Catalysts and Solvents. *Chem. Rev.* **2017**, *117*, 6929–6983. [CrossRef] [PubMed]
66. Karimi, B.; Tavakolian, M.; Akbari, M.; Mansouri, F. Ionic Liquids in Asymmetric Synthesis: An Overall View from Reaction Media to Supported Ionic Liquid Catalysis. *ChemCatChem* **2018**, *10*, 3173–3205. [CrossRef]
67. Kaur, G.; Sharma, A.; Banerjee, B. Ultrasound and Ionic Liquid: An Ideal Combination for Organic Transformations. *ChemistrySelect* **2018**, *3*, 5283–5295. [CrossRef]
68. Nasrollahzadeh, M.; Motahharifar, N.; Sajjadi, M.; Aghbolagh, A.M.; Shokouhimehr, M.; Varma, R.S. Recent advances in N-formylation of amines and nitroarenes using efficient (nano)catalysts in eco-friendly media. *Green Chem.* **2019**, *21*, 5144–5167. [CrossRef]
69. Sotgiu, G.; Chiarotto, I.; Feroci, M.; Orsini, M.; Rossi, L.; Inesi, A. An electrochemical alternative strategy to the synthesis of β-lactams. Part 3. Room-temperature ionic liquids vs molecular organic solvents. *Electrochim. Acta* **2008**, *53*, 7852–7858. [CrossRef]
70. Feroci, M.; Chiarotto, I.; Inesi, A. Electrolysis of ionic liquids. A possible keystone for the achievement of green solvent-catalyst systems. *Curr. Org. Chem.* **2013**, *17*, 204–219. [CrossRef]
71. D'Anna, F.; Marullo, S.; Vitale, P.; Noto, R. The Effect of the Cation π-Surface Area on the 3D Organization and Catalytic Ability of Imidazolium-Based Ionic Liquids. *Eur. J. Org. Chem.* **2011**, *2011*, 5681–5689. [CrossRef]
72. D'Anna, F.; Marullo, S.; Noto, R. Aryl Azides Formation Under Mild Conditions: A Kinetic Study in Some Ionic Liquid Solutions. *J. Org. Chem.* **2010**, *75*, 767–771. [CrossRef]
73. D'Anna, F.; Marullo, S.; Vitale, P.; Noto, R. Synthesis of aryl azides: A probe reaction to study the synergetic action of ultrasounds and ionic liquids. *Ultrason. Sonochem.* **2012**, *19*, 136–142. [CrossRef] [PubMed]
74. Marullo, S.; D'Anna, F.; Rizzo, C.; Noto, R. The ultrasounds–ionic liquids synergy on the copper catalyzed azide–alkyne cycloaddition between phenylacetylene and 4-azidoquinoline. *Ultrason. Sonochem.* **2015**, *23*, 317–323. [CrossRef] [PubMed]
75. Rizzo, C.; D'Anna, F.; Marullo, S.; Noto, R. Task Specific Dicationic Ionic Liquids: Recyclable Reaction Media for the Mononuclear Rearrangement of Heterocycles. *J. Org. Chem.* **2014**, *79*, 8678–8683. [CrossRef] [PubMed]
76. Pandolfi, F.; Feroci, M.; Chiarotto, I. Role of anion and cation in the 1-methyl-3-butylimidazolium ionic liquids BMImX: The Knoevenagel condensation. *ChemistrySelect* **2018**, *3*, 4745–4749. [CrossRef]
77. Pandolfi, F.; Chiarotto, I.; Mattiello, L.; Petrucci, R.; Feroci, M. Two different selective ways in the deprotonation of β-bromopropionanilides: β-lactams or acrylanilides formation. *ChemistrySelect* **2019**, *4*, 12871–12874. [CrossRef]
78. Chiarotto, I.; Feeney, M.M.M.; Feroci, M.; Inesi, A. Electrogenerated N-heterocyclic carbene: N-acylation of chiral oxazolidin-2-ones in ionic liquids. *Electrochim. Acta* **2009**, *54*, 1638–1644. [CrossRef]

79. Chiarotto, I.; Feroci, M.; Orsini, M.; Sotgiu, G.; Inesi, A. Electrogenerated N-heterocyclic carbene: N-functionalization of benzoxazolones. *Tetrahedron* **2009**, *65*, 3704–3710. [CrossRef]
80. Feroci, M.; Elinson, M.N.; Rossi, L.; Inesi, A. The double role of ionic liquids in organic electrosynthesis: Precursors of N-heterocyclic carbenes and green solvents. Henry reaction. *Electrochem. Commun.* **2009**, *11*, 1523–1526. [CrossRef]
81. Feroci, M.; Chiarotto, I.; Vecchio Ciprioti, S.; Inesi, A. On the reactivity and stability of electrogenerated N-heterocyclic carbene in parent 1-butyl-3-methylimidazolium tetrafluoroborate: Formation and use of N-heterocyclic carbene-CO_2 adduct as latent catalyst. *Electrochim. Acta* **2013**, *109*, 95–101. [CrossRef]
82. Feroci, M.; Chiarotto, I.; D'Anna, F.; Gala, F.; Noto, R.; Ornano, L.; Zollo, G.; Inesi, A. N-Heterocyclic carbenes and parent cations: Acidity, nucleophilicity, stability, and hydrogen bonding-electrochemical study and ab initio calculations. *ChemElectroChem* **2016**, *3*, 1133–1141. [CrossRef]
83. Chiarotto, I.; Mattiello, L.; Pandolfi, F.; Rocco, D.; Feroci, M. NHC in imidazolium acetate ionic liquids: Actual or potential presence? *Front. Chem.* **2018**, *6*, 355. [CrossRef] [PubMed]
84. Ali, F.I.M.; Awwad, F.; Greish, Y.E.; Abu-Hani, A.F.S.; Mahmoud, S.T. Fabrication of low temperature and fast response H_2S gas sensor based on organic-metal oxide hybrid nanocomposite membrane. *Org. Electron.* **2020**, *76*, 105486. [CrossRef]
85. Bahadori, M.; Tangestaninejad, S.; Bertmer, M.; Moghadam, M.; Mirkhani, V.; Mohammadpoor−Baltork, I.; Kardanpour, R.; Zadehahmadi, F. Task-Specific Ionic Liquid Functionalized–MIL–101(Cr) as a Heterogeneous and Efficient Catalyst for the Cycloaddition of CO_2 with Epoxides Under Solvent Free Conditions. *ACS Sustain. Chem. Eng.* **2019**, *7*, 3962–3973. [CrossRef]
86. Eyckens, D.J.; Champion, M.E.; Fox, B.L.; Yoganantharajah, P.; Gibert, Y.; Welton, T.; Henderson, L.C. Solvate Ionic Liquids as Reaction Media for Electrocyclic Transformations. *Eur. J. Org. Chem.* **2016**, *2016*, 913–917. [CrossRef]
87. Eyckens, D.J.; Demir, B.; Walsh, T.R.; Welton, T.; Henderson, L.C. Determination of Kamlet–Taft parameters for selected solvate ionic liquids. *Phys. Chem. Chem. Phys.* **2016**, *18*, 13153–13157. [CrossRef]
88. Lui, M.Y.; Crowhurst, L.; Hallett, J.P.; Hunt, P.A.; Niedermeyer, H.; Welton, T. Salts dissolved in salts: Ionic liquid mixtures. *Chem. Sci.* **2011**, *2*, 1491–1496. [CrossRef]
89. Dupont, J. From Molten Salts to Ionic Liquids: A "Nano" Journey. *Acc. Chem. Res.* **2011**, *44*, 1223–1231. [CrossRef]
90. Dupont, J.; Suarez, P.A.Z. Physico-chemical processes in imidazolium ionic liquids. *Phys. Chem. Chem. Phys.* **2006**, *8*, 2441–2452. [CrossRef]
91. Carvalho, T.O.; Carvalho, P.H.P.R.; Correa, J.R.; Guido, B.C.; Medeiros, G.A.; Eberlin, M.N.; Coelho, S.E.; Domingos, J.B.; Neto, B.A.D. Palladium Catalyst with Task-Specific Ionic Liquid Ligands: Intracellular Reactions and Mitochondrial Imaging with Benzothiadiazole Derivatives. *J. Org. Chem.* **2019**, *84*, 5118–5128. [CrossRef]
92. Qian, W.; Tan, X.; Su, Q.; Cheng, W.; Xu, F.; Dong, L.; Zhang, S. Transesterification of Isosorbide with Dimethyl Carbonate Catalyzed by Task-Specific Ionic Liquids. *ChemSusChem* **2019**, *12*, 1169–1178. [CrossRef]
93. Xie, W.; Shao, L. Phosphorylation of Corn Starch in an Ionic Liquid. *Starch/Stärke* **2009**, *61*, 702–708. [CrossRef]
94. El Sayed, S.; Bordet, A.; Weidenthaler, C.; Hetaba, W.; Luska, K.L.; Leitner, W. Selective Hydrogenation of Benzofurans Using Ruthenium Nanoparticles in Lewis Acid-Modified Ruthenium-Supported Ionic Liquid Phases. *ACS Catal.* **2020**, *10*, 2124–2130. [CrossRef]
95. Fatehi, A.; Ghorbani-Vaghei, R.; Alavinia, S.; Mahmoodi, J. Synthesis of Quinazoline Derivatives Catalyzed by a New Efficient Reusable Nanomagnetic Catalyst Supported with Functionalized Piperidinium Benzene-1,3-Disulfonate Ionic Liquid. *ChemistrySelect* **2020**, *5*, 944–951. [CrossRef]
96. Zhao, Q.; Yang, C.; Fang, M.; Jiang, T. Performance of Brönsted-Lewis acidic ionic liquids supported Ti-SBA-15 for the esterification of acetic acid to benzyl alcohol. *Appl. Catal. A General* **2020**, *594*, 117470. [CrossRef]
97. Billeci, F.; D'Anna, F.; Gunaratne, H.Q.N.; Plechkova, N.V.; Seddon, K.R. "Sweet" ionic liquid gels: Materials for sweetening of fuels. *Green Chem.* **2018**, *20*, 4260–4276. [CrossRef]
98. Guo, P.; Su, A.; Wei, Y.; Liu, X.; Li, Y.; Guo, F.; Li, J.; Hu, Z.; Sun, J. Healable, Highly Conductive, Flexible, and Nonflammable Supramolecular Ionogel Electrolytes for Lithium-Ion Batteries. *ACS Appl. Mater. Interfaces* **2019**, *11*, 19413–19420. [CrossRef] [PubMed]

99. Kuddushi, M.; Mata, J.; Malek, N. Self-Sustainable, self-healable, Load Bearable and Moldable stimuli responsive ionogel for the Selective Removal of Anionic Dyes from aqueous medium. *J. Mol. Liq.* **2020**, *298*, 112048. [CrossRef]
100. Marullo, S.; Rizzo, C.; Dintcheva, N.T.; Giannici, F.; D'Anna, F. Ionic liquids gels: Soft materials for environmental remediation. *J. Colloid Interface Sci.* **2018**, *517*, 182–193. [CrossRef]
101. Rizzo, C.; Marullo, S.; Campodonico, P.R.; Pibiri, I.; Dintcheva, N.T.; Noto, R.; Millan, D.; D'Anna, F. Self-Sustaining Supramolecular Ionic Liquid Gels for Dye Adsorption. *ACS Sustain. Chem. Eng.* **2018**, *6*, 12453–12462. [CrossRef]
102. Billeci, F.; D'Anna, F.; Feroci, M.; Cancemi, P.; Feo, S.; Forlino, A.; Tonnelli, F.; Seddon, K.R.; Gunaratne, H.Q.N.; Plechkova, N.V. When Functionalization Becomes Useful: Ionic Liquids with a "Sweet" Appended Moiety Demonstrate Drastically Reduced Toxicological Effects. *ACS Sustain. Chem. Eng.* **2020**, *8*, 926–938. [CrossRef]
103. Egorova, K.S.; Ananikov, V.P. Toxicity of Ionic Liquids: Eco(cyto)activity as Complicated, but Unavoidable Parameter for Task-Specific Optimization. *ChemSusChem* **2014**, *7*, 336–360. [CrossRef] [PubMed]
104. Hulsbosch, J.; De Vos, D.E.; Binnemans, K.; Ameloot, R. Biobased Ionic Liquids: Solvents for a Green Processing Industry? *ACS Sustain. Chem. Eng.* **2016**, *4*, 2917–2931. [CrossRef]
105. Socha, A.M.; Parthasarathi, R.; Shi, J.; Pattathil, S.; Whyte, D.; Bergeron, M.; George, A.; Tran, K.; Stavila, V.; Venkatachalam, S.; et al. Efficient biomass pretreatment using ionic liquids derived from lignin and hemicellulose. *Proc. Natl. Acad. Sci. USA* **2014**, *111*, E3587–E3595. [CrossRef] [PubMed]
106. Worlds Health Organization (WHO). Health Topics. Available online: https://www.who.int/health-topics/air-pollution#tab=tab_1 (accessed on 14 February 2020).
107. Worlds Health Organization (WHO). Available online: https://www.who.int/airpollution/ambient/pollutants/en/) (accessed on 14 February 2020).
108. Duk-Dong, L.; Dae-Sik, L. Environmental gas sensors. *IEEE Sensors J.* **2001**, *1*, 214–224. [CrossRef]
109. Rai, A.C.; Kumar, P.; Pilla, F.; Skouloudis, A.N.; Di Sabatino, S.; Ratti, C.; Yasar, A.; Rickerby, D. End-user perspective of low-cost sensors for outdoor air pollution monitoring. *Sci. Total Environ.* **2017**, *607–608*, 691–705. [CrossRef]
110. Pang, X.; Shaw, M.D.; Gillot, S.; Lewis, A.C. The impacts of water vapour and co-pollutants on the performance of electrochemical gas sensors used for air quality monitoring. *Sens. Actuators B Chem.* **2018**, *266*, 674–684. [CrossRef]
111. Moseley, P.T. Progress in the development of semiconducting metal oxide gas sensors: A review. *Meas. Sci. Technol.* **2017**, *28*, 082001. [CrossRef]
112. Dong, C.; Zhao, R.; Yao, L.; Ran, Y.; Zhang, X.; Wang, Y. A review on WO_3 based gas sensors: Morphology control and enhanced sensing properties. *J. Alloys Compd.* **2020**, *820*, 153194. [CrossRef]
113. Hariharan, V.; Gnanavel, B.; Sathiyapriya, R.; Aroulmoji, V.A. A Review on Tungsten Oxide (WO_3) and their Derivatives for Sensor Applications. *Int. J. Adv. Sci. Eng.* **2019**, *5*, 1163–1168. [CrossRef]
114. Sari, W.P.; Leigh, S.; Covington, J. Tungsten Oxide Based Sensor for Oxygen Detection. *Proceedings* **2018**, *2*, 952. [CrossRef]
115. Staerz, A.; Somacescu, S.; Epifani, M.; Russ, T.; Weimar, U.; Barsan, N. WO_3 Based Gas Sensors. *Proceedings* **2018**, *2*, 826. [CrossRef]
116. Li, Z.; Li, J.; Song, L.; Gong, H.; Niu, Q. Ionic liquid-assisted synthesis of WO_3 particles with enhanced gas sensing properties. *J. Mat. Chem. A* **2013**, *1*, 15377–15382. [CrossRef]
117. Zhang, Y.; Cheng, X.; Zhang, X.; Major, Z.; Xu, Y.; Gao, S.; Zhao, H.; Huo, L. Ionic liquid-assisted synthesis of tungsten oxide nanoparticles with enhanced NO_2 sensing properties at near room temperature. *Appl. Surf. Sci.* **2020**, *505*, 144533. [CrossRef]
118. Favard, A.Y.X.; Anguille, S.; Moulin, P.; Seguin, J.-L.; Aguir, K.; Bendahan, M. Ionic Liquids Filter for Humidity Effect Reduction on Metal Oxide Gas Sensor Response. *Sensors Transduc.* **2018**, *222*, 6–11.
119. Abu-Hani, A.F.S.; Awwad, F.; Greish, Y.E.; Ayesh, A.I.; Mahmoud, S.T. Design, fabrication, and characterization of low-power gas sensors based on organic-inorganic nano-composite. *Org. Electron.* **2017**, *42*, 284–292. [CrossRef]
120. Daves, W.; Ersoez, B. Electrochemical Gas Sensor. International Patent Application No. WO2018/234185 A1, 27 December 2018.
121. Bhutto, A.W.; Abro, R.; Gao, S.; Abbas, T.; Chen, X.; Yu, G. Oxidative desulfurization of fuel oils using ionic liquids: A review. *J. Taiwan Inst. Chem. Eng.* **2016**, *62*, 84–97. [CrossRef]

122. Daage, M.; Chianelli, R.R. Structure-Function Relations in Molybdenum Sulfide Catalysts: The "Rim-Edge" Model. *J. Catal.* **1994**, *149*, 414–427. [CrossRef]
123. Topsøe, H. The role of Co–Mo–S type structures in hydrotreating catalysts. *Appl. Catal. A General* **2007**, *322*, 3–8. [CrossRef]
124. Shan, S.; Yuan, P.; Han, W.; Shi, G.; Bao, X. Supported NiW catalysts with tunable size and morphology of active phases for highly selective hydrodesulfurization of fluid catalytic cracking naphtha. *J. Catal.* **2015**, *330*, 288–301. [CrossRef]
125. Hossain, M.N.; Park, H.C.; Choi, H.S. A Comprehensive Review on Catalytic Oxidative Desulfurization of Liquid Fuel Oil. *Catalyst* **2019**, *9*, 12. [CrossRef]
126. Sun, H.; Wu, P.; He, J.; Liu, M.; Zhu, L.; Zhu, F.; Chen, G.; He, M.; Zhu, W. Fabrication of oxygen-defective tungsten oxide nanorods for deep oxidative desulfurization of fuel. *Pet. Sci.* **2018**, *15*, 849–856. [CrossRef]
127. Rongxiang, Z.; Xiuping, L.; Jianxun, S.; Weiwei, S.; Xiaohan, G. Preparation of WO_3/C Composite and Its Application in Oxidative Desulfurization of Fuel. *China Pet. Process. Petrochem. Technol.* **2017**, *19*, 65–73.
128. Li, X.; Zhao, R.; Mao, C. Polycrystalline Phase WO_3/g-C_3N_4 as a High Efficient Catalyst for Removal of DBT in Model Oil. *China Pet. Process. Petrochem. Technol.* **2019**, *21*, 36–45.
129. Zhang, M.; Zhu, W.; Li, H.; Xun, S.; Li, M.; Li, Y.; Wei, Y.; Li, H. Fabrication and characterization of tungsten-containing mesoporous silica for heterogeneous oxidative desulfurization. *Chin. J. Catal.* **2016**, *37*, 971–978. [CrossRef]
130. Xun, S.; Hou, C.; Li, H.; He, M.; Ma, R.; Zhang, M.; Zhu, W.; Li, H. Synthesis of WO_3/mesoporous ZrO_2 catalyst as a high-efficiency catalyst for catalytic oxidation of dibenzothiophene in diesel. *J. Mat. Sci.* **2018**, *53*, 15927–15938. [CrossRef]
131. Ma, R.; Guo, J.; Wang, D.; He, M.; Xun, S.; Gu, J.; Zhu, W.; Li, H. Preparation of highly dispersed WO_3/few layer g-C_3N_4 and its enhancement of catalytic oxidative desulfurization activity. *Colloid. Surface. A: Physicochem. Eng. Aspects* **2019**, *572*, 250–258. [CrossRef]
132. Wang, C.; Li, A.; Xu, J.; Wen, J.; Zhang, H.; Zhang, L. Preparation of WO_3/CNT catalysts in presence of ionic liquid [C_{16}mim]Cl and catalytic efficiency in oxidative desulfurization. *J. Chem. Technol. Biotechnol.* **2019**, *94*, 3403–3412. [CrossRef]